M. V. Casterline, C. Salvaggio, A. J. Garrett, J. W. Faulring, B. D. Bartlett, and P. S. Salvaggio, "Improved temperature retrieval methods for the validation of a hydrodynamic simulation of a partially frozen power plant cooling lake," in *Proceedings of SPIE, SPIE Defense and Security, Thermosense XXXII, Utilities and Fluid Dynamics*, **7661**, SPIE, (Orlando, Florida, United States), April 2010



http://dx.doi.org/10.1117/12.850280

# Improved temperature retrieval methods for the validation of a hydrodynamic simulation of a partially frozen power plant cooling lake

May V. Casterline[a], Carl Salvaggio[a], Alfred J. Garrett[b], Brent D. Bartlett[a], Jason W. Faulring[c], and Philip S. Salvaggio[a]

[a] Rochester Institute of Technology, Center for Imaging Science, Digital Imaging and Remote Sensing Laboratory, Rochester, New York, USA
[b] Savannah River National Laboratory, Aiken, South Carolina, USA
[c] Rochester Institute of Technology, Center for Imaging Science, Laboratory for Imaging Algorithms and Systems, Rochester, New York, USA

## ABSTRACT

The ALGE code is a hydrodynamic model developed by Savannah River National Laboratory (SRNL) to derive the power output levels of an electric generation facility from observing the associated cooling pond with an aerial imaging platform. Over the past two years work has been completed to extend the capabilities of the model to incorporate snow and ice as possible phenomena in the modeled environment. In order to validate the extension of the model, intensive ground truth data as well as high-resolution aerial infrared imagery were collected during the winters of 2008-2009 and 2009-2010, for a combined eight months of data collection. Due to the harsh and extreme environmental conditions automatic data collection instruments were designed and deployed. Based on experience gained during the first collection season and equipment design failures, overhauls in the design and operation of the automated data collection buoys were performed. In addition, a more thorough and robust two-fold calibration technique was implemented within the aerial imaging chain to assess the accuracy of the retrieved surface temperatures. By design, the calibration method employed in this application uses ground collected, geo-located water surface temperatures and in-flight blackbody imagery to produce accurate temperature maps of the pond in interest. A sensitivity analysis was implemented within the data reduction technique to produce accurate sensor reaching temperature values using designed equipment and methods for temperature retrieval at the water's surface.

**Keywords:** thermal infrared, hydrodynamic modeling, simulation, ice, snow, ground truth, thermal calibration, remote sensing, ice thickness

## 1. INTRODUCTION

The ALGE code is a hydrodynamic model developed by Savannah River National Laboratory (SRNL) to derive the power output levels of a power generation site from observing the site's associated cooling pond with an aerial imaging platform. This research is funded by the United States Department of Energy with the objective of improving our ability to understand and simulate the thermodynamics and hydrodynamics of power plant cooling lakes when they are partially frozen. When a site is located in a northern climate, the waste heat entering the cooling lake is often not enough to keep the lake from freezing during winter months. Once the lake is partially or fully frozen, the predictive capability of the original version of the hydrodynamic model was weakened due to the insulating surface layer of ice and snow. Based on data acquired during the 2008-2009 winter, improvements were made to ALGE to add the ability to account for ice and snow formation on a pond's surface.[1] To further refine the modeling capabilities, another data collection campaign was planned and implemented for the winter of 2009-2010. As part of this refinement process, RIT's WASP airborne imaging system was calibrated to absolute ground temperature using observations made both manually and autonomously, coincident with all airborne collection campaigns.

Further author information: E-mail: mva7609@cis.rit.edu

Thermosense XXXII, edited by Ralph B. Dinwiddie, Morteza Safai, Proc. of SPIE
Vol. 7661, 766106 · © 2010 SPIE · CCC code: 0277-786X/10/$18 · doi: 10.1117/12.850280

The data campaign for the winter of 2009-2010 was segmented into two efforts: the aerial imagery and the ground truth collection. Five autonomous data collection systems (buoys) were reengineered and re-deployed in the cooling lake of the Midland Cogeneration Venture (MCV) located in Midland, Michigan. A weather station was maintained on the shore, and a permanent camera system was mounted on the roof of a MCV facility building to continually monitor the lake surface conditions . The buoys, weather station, and roof-based camera system queried their various instruments automatically and transmitted the data daily via cellular modems to the laboratory at RIT. In addition to the constant monitoring provided by the buoys, manual, surface temperature measurements were taken immediately following imagery collects so not to disturb the surface water conditions when the images were being collected.

A process was developed to translate the raw imagery of the cooling pond, acquired during flight by the longwave infrared camera, into calibrated, geo-referenced, absolute temperature estimates of exposed pond water. In order to accomplish this translation, images were first calibrated to sensor reaching radiance using the on-board blackbody calibrators and then correlated to calibrated, geo-referenced ground temperature measurements. Calibration studies were performed both in the laboratory and in the field on a suite of ground based instruments for measuring water temperature through contact and non-contact methods. In addition, a sensitivity analysis was performed, on a per-pixel basis, to determine the accuracy of the longwave and midwave cameras on the WASP system.

## 2. BACKGROUND AND THEORY

### 2.1 ALGE Model

ALGE is a 3-D hydrodynamic model developed by SRNL as part of the Multi-spectral Thermal Imager (MTI) project.[2] ALGE was originally developed, using thermal imagery as a model input, to simulate power plant discharge waters to cooling lakes and other free surface water bodies (cooling canals, direct discharge to rivers, and ocean). Situations in which ice formation occurred were not considered in the original version of the code. Thermal imagery provides a unique method for observing the thermal waste heat injected into a cooling pond by offering a complete spatial view of the thermal plume at a point in time. Additional required inputs for the simulation are the site specific weather and the cooling pond bathymetry.[3] Figure 1 depicts simulated surface temperature maps for a series of ALGE model runs for the same pond over varying weather conditions.

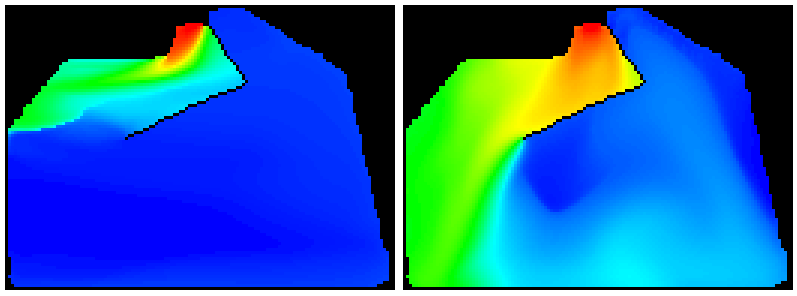

(a) Simulated thermal structure during freeze-up

(b) Simulated thermal structure during warm-up

Figure 1. ALGE surface temperature predictions for the Midland Cogeneration Venture cooling pond in Midland, MI using historical weather information.

The ALGE code optimizes the mass flow rate prediction for a given lake and weather conditions by incrementally changing the power generation facility's operating parameters. The rate at which the thermal waste is discharged into the pond can be used in subsequent engineering process models to predict operating power levels for the power generation site. A predicted thermal plume is output for each combination of parameters and is compared to the observed thermal plume image. The parameters used to produce the thermal plume prediction that is most similar to the observed thermal plume are designated as the hypothesized plant operational parameters.

## 3. GROUND TRUTH SYSTEMS

### 3.1 Autonomous in-situ measurements

Following the challenges of the 2008-2009 collection efforts, a massive overhaul and reengineering of the deployable buoy monitoring systems was completed. The basic construction of the buoys remained unchanged. A Campbell Scientific CR1000 datalogger was mounted inside a weather proof box and used to control all the querying and logging of various instruments mounted to a large dock float. The CR1000 monitored two different deployments of thermocouples used to measure the temperature profile of the water and ice thickness. The temperature profile thermocouples were attached to the mooring chain at one-foot increments and were queried by the datalogger at 30-second intervals. Every five minutes an average temperature value at each thermocouple was calculated and recorded. The second set of thermocouples was attached to an insulated metal pole, at approximately 1-inch increments, beginning at the waterline of the buoy. These high-density thermocouples measured the temperature of either water or ice every 30 seconds with an average temperature recorded every five minutes. In addition to the main measurement systems on the buoys, twelve Tidbit dataloggers are attached to the chain of each buoy to serve as a backup temperature measurement system. Each buoy was also equipped with a cellular modem and RF antenna. Every day, each buoy would come online and transmit a day's worth of collected data back to an automated, web-based database and dissemination system.

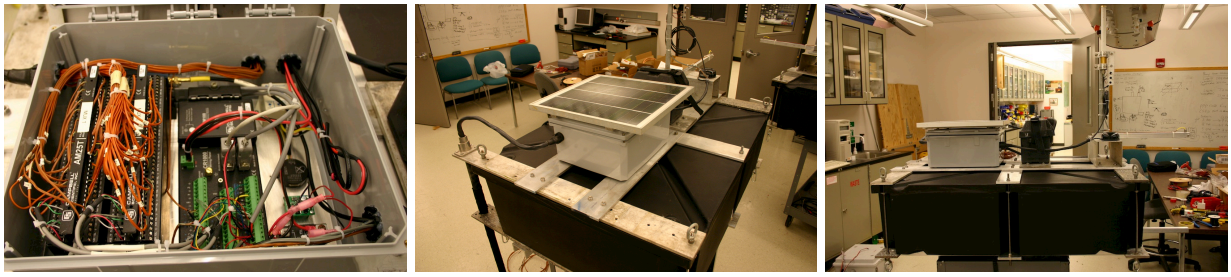

(a) Internal buoy components (b) Externally mounted solar panel (c) Orientation of battery box, antenna, and electronics box

Figure 2. Newly designed buoys

Notable problems from the 2008-2009 winter season included: power failures, communication failures, challenging accessibility issues for maintenance, lack of insight into the actual 3-axis positioning of a given buoy, and lack of a back-up system for collected data. In order to combat the system failures mentioned above, modifications were made to the buoy design as well as the controlling software. The internal components of a newly designed and constructed buoy is show above in Figure 2(a). A compact flash memory card was installed on each buoy to serve as a backup should there be a communication failure. In addition, an accelerometer was added to report on the 3-axis orientation of a given buoy. This added information provided insight into the angle at which a buoy was oriented should it become frozen in the ice. The angle at which a buoy freezes directly affects the extrapolated position of any thermocouple on the ice profiler and, by association, the derived location of an ice/water boundary. In addition to a dynamic mooring chain assembly, the float size and buoyancy rating was increased from 200 lbs buoyancy to 700 lbs buoyancy to increase the platform's resistance to freezing at angles. To address power failure issues, a 12 watt solar panel was mounted to the top of the environmental enclosure and the battery location was moved to an external mount point, shown in Figure 2(b) and Figure 2(c). Each weather proof box containing all electrical components was permanently sealed shut to prevent any water seepage. In case of software failures mid-winter, the capability to manually turn on the modem was added via a toggle switch on the antenna. This added functionality allowed the software and firmware on the datalogger to be modified via a wireless internet connection and alleviated the need to access the datalogger while deployed. Figure 3 shows the buoys successfully deployed in the MCV cooling pond. A single weather station was located near the hot water discharge point on shore. The station is identical to the one used for the previous winter's data campaign.[4]

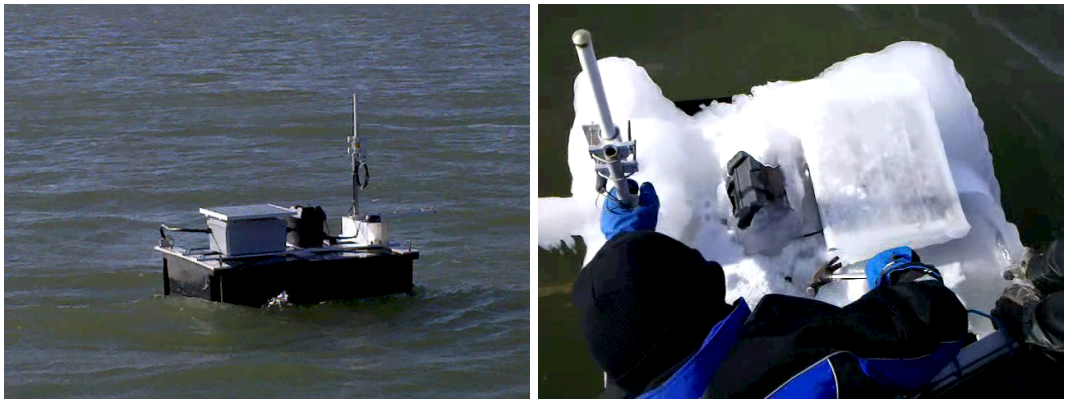

Figure 3. Newly designed buoys afloat in MCV cooling pond

### 3.2 Manual ground truth collection

Data collected by the ground truth team included localized relative humidity, water surface temperature, and bulk water temperature. All ground truth measurements were made from a pontoon boat and were recorded immediately following the collection of aerial imagery. It was not advisable to collect surface temperatures concurrently with the flight due to the thermal influence the boat would have on the surface temperatures of the exposed water. It was assumed there was approximately a one hour window following the imagery collection where any collected surface temperatures were valid. Bulk temperature measurements were made with both a contact thermistor mounted on a styrofoam float and an Omega HH41 temperature probe. Surface temperatures were observed using both an Omega OS36 infrared radiometer and a Heitronics KT19.82 infrared radiometer. Positioning information was recorded using a handheld Garmin E-Trax GPS and localized weather data (i.e. relative humidity and wind speed) was collected using a handheld Kestrel 4000 weather meter.

## 4. AERIAL IMAGERY COLLECTION

### 4.1 RIT's WASP Sensor

RIT's Wildfire Airborne Sensor Program (WASP) instrument, shown in Figure 4, is a multispectral aerial mapping system with broadband coverage in the infrared and visible spectrum. Built by the RIT Laboratory for Imaging Algorithms and Systems (LIAS), WASP utilizes direct georeferencing hardware and processing techniques to create orthorectified imagery on-the-fly as the sensor is flown over the target scene. A recent upgrade to the system has enabled the generation of calibrated midwave and longwave infrared imagery.

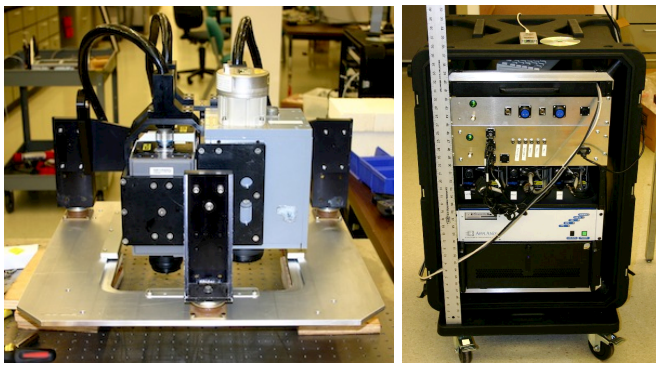

Figure 4. WASP sensor in laboratory

Originally designed as a wild fire detection and mapping system, WASP was built with three 640x512 pixel infrared cameras covering 0.9 -1.7$\mu m$, 3-5$\mu m$ and 8-9.2$\mu m$; this spectral coverage allows the use a multispectral technique for positively detecting the presence of a wildfire in the imaged scene. Each infrared (IR) camera

has a 25 micron pixel pitch and a lens with an approximate focal length of 25mm. The system also carries a 4000x2672 pixel RGB camera with a 9 micron pixel pitch and 50mm lens; this camera provides higher resolution visual coverage of the mission area. While not metric by design, each camera's optical system is stabilized for flight conditions and is geometrically modeled for lens distortion, principle point offsets, and focal length. To enable the creation of orthophotos by direct georeferencing, an Applanix POSAV-310 is utilized to record attitude information during the mission's flight. The POS's Litton LN-200 inertial measurement unit (IMU) is rigidly mounted to the camera frame assembly and boresight alignment angles for each camera are applied to generate exterior orientation parameters for each exposure station. Boresight angles for each camera are developed through a traditional bundle adjustment process utilizing highly-overlapped imagery, flown over a surveyed control point field.

All imagery and metadata from the mission flight are recorded by a rack-mounted computer system on solid state removable media allowing for a service ceiling of at least 20,000 feet (tested) and high reliability without the use of specialized sealed hard drive enclosures. The WASP automated data processing computer (ADP) has the ability to orthorectify imagery on-the-fly as it's collected utilizing real-time exterior orientation solutions calculated by the POS and an archived digital elevation model of the area. Real-time generated orthos typically tie together acceptably for tactical applications and are absolutely accurate to about 4 meters rms; this data can be transmitted to ground observers via a high bandwidth RF data link. Once the plane lands, the raw recorded data can be further refined in a post-processing workflow yielding directly georeferenced ortho images absolutely accurate to better than 0.5 meters rms.

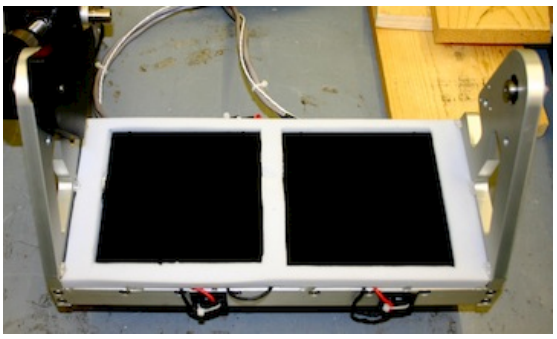

(a) Both blackbody sources

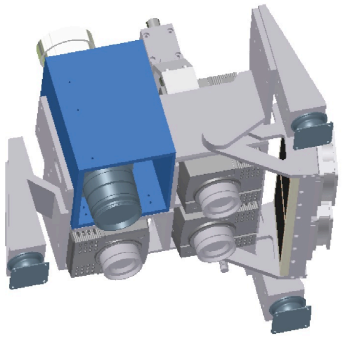

(b) AutoCAD image of WASP with blackbodies

Figure 5. WASP sensor with blackbody reference sources.

MWIR and LWIR array cameras are inherently susceptible to changes in environment that manifest as non-uniformities in the collected imagery. Most commercial IR camera systems provide mechanisms to perform uniformity corrections in a fixed environment; these procedures are not practical when applied to a constantly changing environment aboard an aircraft. Two thermoelectric plate blackbody reference sources are included to address these issues. During a typical flight, the calibrators are moved to fill the field-of-view of the camera and imaged at two temperatures that bracket the expected temperatures in the scene to be mapped, typically at the beginning and end of a flight line. Imagery and temperatures gathered during the calibration process are used to post process imagery from the MWIR and LWIR cameras to perform a non-uniformity correction and calibrate the images to sensor reaching radiance. The blackbody sources and their configuration on WASP are shown in Figures 5(a) and 5(b).

## 5. CALIBRATION TECHNIQUES

### 5.1 WASP sensor calibration methodology

Raw data from both the LWIR and MWIR detectors are written out as 14-bit ITTVIS ENVI format images. In order to minimize projection affects and preserve the radiometric integrity of the raw data contained in these images, the conversion from digital number to radiance units is performed prior to the georeferencing process.

Additionally, due to a significant non-uniformity across the LWIR focal plane and variable readout gain visible in the MWIR plane, each image is calibrated to sensor-reaching radiance on a pixel-by-pixel basis.

For most aerial collections blackbody imagery is collected at the beginning and end of each flight line. Each reference source is driven to either a hot or cold set point and moved to fill the field of view for both sensors simultaneously. The hot and cold set points are chosen to adequately bracket the scene's thermal content of interest. After the first reference source imagery collection (at either a hot or cold set point), the blackbodies are driven to the opposite end of the thermal range during the imagery acquisition over the scene, and then re-introduced into the field of view while the aircraft is making a turn. Figure 6(a) is a conceptual example for how this type of imagery collection scheme is implemented. The sources have been tested and are known to be radiating at a uniform, measurable temperature across the surface of the blackbody

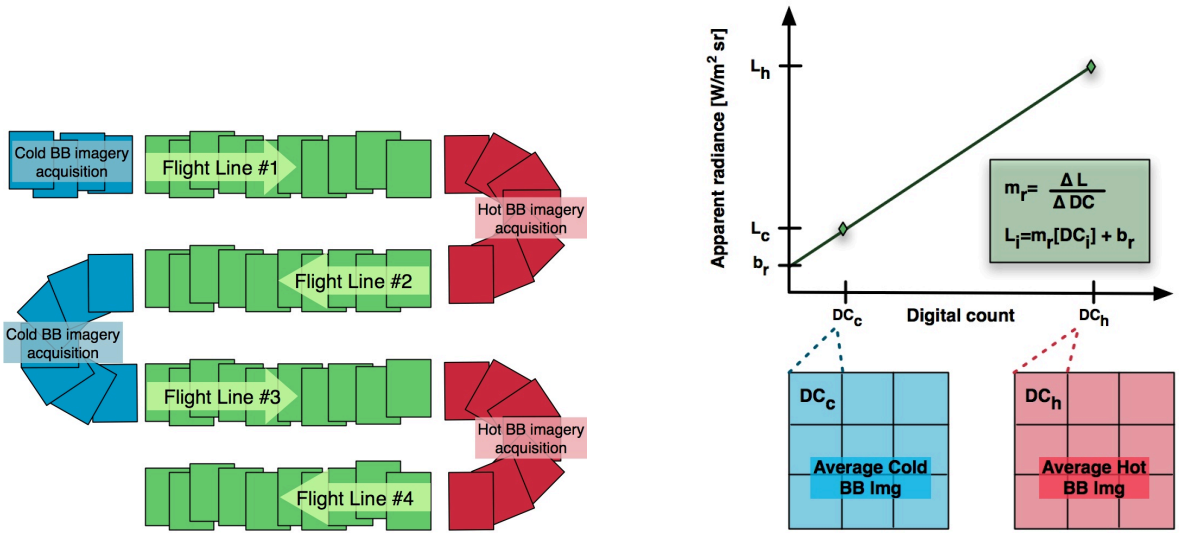


(a) Flight line collection scheme for blackbody imagery collection during flight

(b) Digital count to radiance conversion

Figure 6. Collection and usage of in-flight reference source imagery

Each collection of reference source imagery is temporally averaged to reduce noise during collection. Prior to any radiometric calculation, an analysis is performed to identify and interpolate any dead pixels on the detector's focal plane. It is assumed that 0.05% of the total number of pixels are dead. Using the histogram statistics for a given average blackbody image, the top 0.025% and bottom 0.025% of pixels are designated as dead pixels and are filled with a bi-linear interpolation of neighboring pixel values.

Given the known spectral emissivity of the blackbody material, the spectral response of each of the WASP thermal cameras, and the measured temperature of blackbody during image acquisition, the total radiance emitted by the reference source is determined by integrating the Planck blackbody equation over the spectral range of the WASP detector. This calculation is performed for both the hot- and cold-averaged blackbody images. For each flight, the digital count values at every pixel for both the hot- and cold-averaged blackbody images is related to the calculated total emitted radiance from the reference sources using a linear regression model. Due to the fact that the set points for the reference sources were chosen based on the thermal content of target scene, the gain ($m_r$) and bias ($b_r$) calculated for each pixel will generate an apparent sensor reaching radiance value for any given digital count acquired while imaging the scene (Figure 6(b)). The end result of this process are gain and bias masks for each flight line. These masks are applied to each image acquired during a flight line to convert the raw data into apparent sensor reaching radiance. Following this conversion, image tiles are geo-referenced and stitched together to create a single image mosaic encompassing the entire scene of interest.

In order to compensate for atmospheric effects and correlate to apparent ground temperature, geo-referenced ground truth measurements of the target (water surface) were collected. Both skin and bulk temperature

measurements of the water were recorded, however, the skin temperature measurements were used for calibration efforts. The choice to use only skin temperature measurements was made because a skin temperature model would have needed to be implemented to convert bulk measurements to surface measurements. None of the models research adequately handled the highly dynamic environment observed on the cooling pond.

Using the map coordinates associated with each measurement, the corresponding calculated radiance value was extracted from the georeferenced, sensor-reaching radiance mosaic. It was assumed that over the range of temperatures investigated and using the WASP system, the relationship between sensor-reaching apparent radiance and target temperature was linear. To confirm that not only a linear relationship was maintained over the entire thermal range, but also over the smaller range of actual target temperatures, the total emitted radiance for a water target at a given temperature, as observed by the WASP LWIR detector, was calculated. The relationship between temperature and radiance is demonstrated below in Figure 7. It should be noted that when fit with a linear model, the gain and bias remain relatively unchanged for both the full thermal range and the subset.

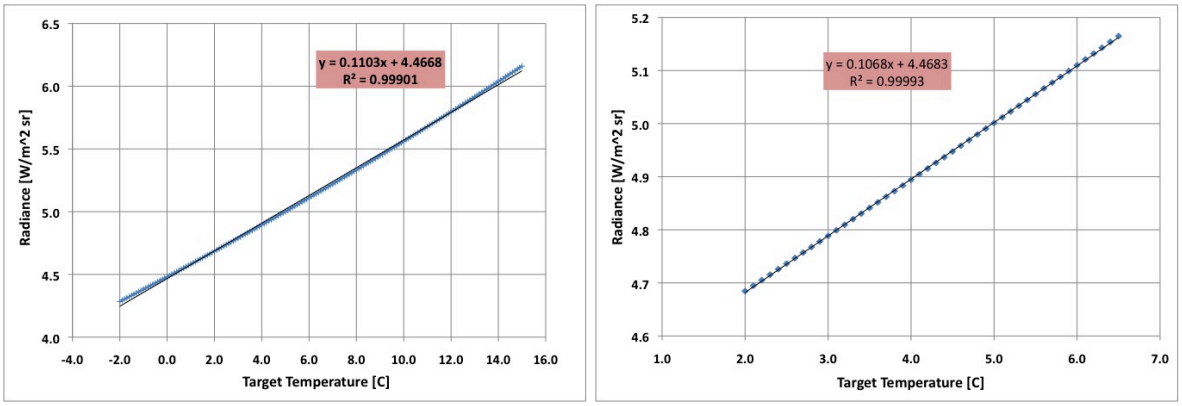


(a) Linear relationship between radiance and temperature for entire range possible scene temperatures

(b) Linear relationship between radiance and temperature for subset of thermal range of possible scene temperatures

Figure 7. Confirmation of linear relationship assumption between sensor-reaching radiance and ground temperature

An additional step was taken to calibrate the instrument-acquired measurements to actual temperature using instrument calibration data acquired in the field. A Heitronics KT19.82 radiometer and Omega OS36 radiometer were used to collect skin temperature measurements for the results presented. Calibration points were collected using a portable Omega blackbody calibration source that was driven to temperatures that thermally bracketed the water targets to be measured. A linear model was used to generate a gain ($m_c$) and bias ($b_c$) to be used to convert observed temperatures to absolute temperatures.

The calibrated, ground-collected, skin temperature measurements were then compared to the geographically tagged sensor-reaching radiance values. All radiance values are corrected for the water target emissivity ($\epsilon = 0.987$). Based on the aforementioned linear relationship assumption, a linear model was fit to the radiance-temperature data pairs, producing a gain ($m_g$) and bias ($b_g$) that is used convert from sensor-reaching apparent radiance to the ground temperature of water at a given location. The relationship between the radiance temperature pairs is depicted below in Figure 8. It is important to note that all derived ground temperatures are only valid for water.

### 5.2 WASP sensor sensitivity analysis

Given a governing equation, the propagation of errors by independent variables can be determined by calculating the total differential of the function. For example, given a function $V = f(x, y)$, the total variance in $V$, $\sigma_V^2$, can be calculated using Equation 1 where $\rho_{xy}$ is the correlation coefficient between the two variables.[5]

$$\sigma_V^2 = \left(\frac{\delta V}{\delta x}\right)^2 \sigma_x^2 + \left(\frac{\delta V}{\delta y}\right)^2 \sigma_y^2 + 2\rho_{xy}\left(\frac{\delta V}{\delta x}\right)\left(\frac{\delta V}{\delta y}\right)\sigma_x\sigma_y \quad (1)$$

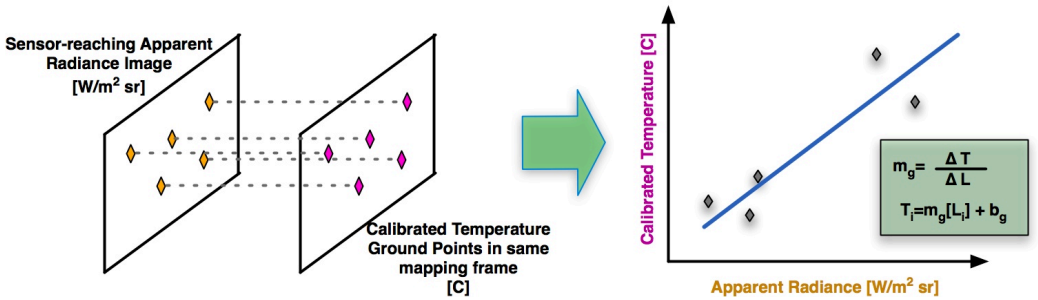


Figure 8. Apparent sensor-reaching radiance to temperature conversion

The entire process of conversion from digital number to absolute ground temperature (water only) can be described using a single governing equation (Equation 2) based on all the linear regression models used to determine the final temperature. Because the conversion from digital count to sensor-reaching radiance was performed on a pixel-by-pixel basis, a temperature is derived for every pixel using a unique $m_r$ and $b_r$. The governing equation is derived from a series of linear regression models fit to well-calibrated physical data and applied in sequential order and therefore all variables are considered independent and uncorrelated.

$$T_{cal_{i,j}} = m_c m_g m_{r_{i,j}} [DC_{WASP_{i,j}}] + m_c m_g b_{r_{i,j}} + m_c b_g + b_c \tag{2}$$

Applying Equation 1 to Equation 2 produces the formula (Equation 3) for determining the variance in a produced temperature map of the water on a pixel-by-pixel basis. The variables are independent and uncorrelated so the last term in Equation 1 can be ignored. The final variance measure will have the same units as the governing equation (temperature). It is important to note that because the temperature is calculated on a pixel-by-pixel basis a variance will be calculated for every pixel, generating a corresponding error map for each temperature map generated.

$$\begin{aligned} \sigma^2_{T_{cal_{i,j}}} &= \left(\frac{\delta T_{cal}}{\delta m_c}\right)^2 \sigma^2_{m_c} + \left(\frac{\delta T_{cal}}{\delta m_g}\right)^2 \sigma^2_{m_g} + \left(\frac{\delta T_{cal}}{\delta m_{r_{i,j}}}\right)^2 \sigma^2_{m_{r_{i,j}}} \\ &+ \left(\frac{\delta T_{cal}}{\delta raw_{i,j}}\right)^2 \sigma^2_{raw_{i,j}} + \left(\frac{\delta T_{cal}}{\delta b_{r_{i,j}}}\right)^2 \sigma^2_{b_{r_{i,j}}} + \left(\frac{\delta T_{cal}}{\delta b_g}\right)^2 \sigma^2_{b_g} + \left(\frac{\delta T_{cal}}{\delta b_c}\right)^2 \sigma^2_{b_c} \end{aligned} \tag{3}$$

### 5.3 Ground instrument calibration

Field instruments (Heitronics KT19.82 radiometer and Omega OS36 radiometer) were calibrated in the field using a portable blackbody. However, all on-board instrumentation built into the buoys was calibrated, pre-deployment, using controlled thermal conditions in the laboratory.

The temperature profiling thermocouples attached to the chain of the buoys were calibrated by placing the entire buoy system inside a walk-in cooler with temperature control. While the thermocouple measured temperatures were recorded, the on-board radiometer (also an Omega OS36) was positioned so that its field of view was filled by a CI Systems infrared blackbody source. The internal air temperature of the cooler was set at three different set-points, the bracketing limits of which were dictated by humidity levels inside the cooler to avoid condensation. When a set point was reached inside the chamber, the blackbody reference source was driven to a range of temperatures and the observed surface temperature, by the on-board radiometer, was recorded.

Because the thermocouples imbedded in the ice profiler are affixed to an aluminum rod, encased in shrink wrap, the thermal inertia inherent to this design prevented the profiler thermocouples from being calibrated using the same method as the chain thermocouples. Instead, the ice profiler was immersed in a controlled-temperature water bath. Both of these calibration processes were repeated for all five buoys that were deployed in the cooling pond.

## 6. RESULTS

Two sets of data were calibrated using the aforementioned process (Sections 5.1 and 5.2). Both data sets were acquired at night, however the water surface temperature data acquired during the 11 February 2010 collect was measured using the Heitronics KT19.82 radiometer while the data acquired during the 4 March 2010 collect was measured using the Omega OS36 radiometer. Shown below in Figure 9 are the calibration data collected during both evenings in the field and applied to all temperature measurements.

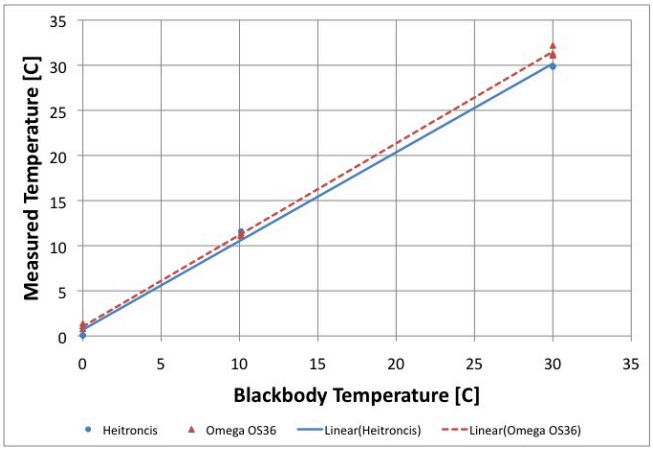


Figure 9. Field collected calibration data for both ground truth infrared radiometers.

Each data set was processed to generate both temperature maps (Figure 10) and error maps. Derived temperatures are only valid for water and each pixel's error is designated by the corresponding per-pixel error map.

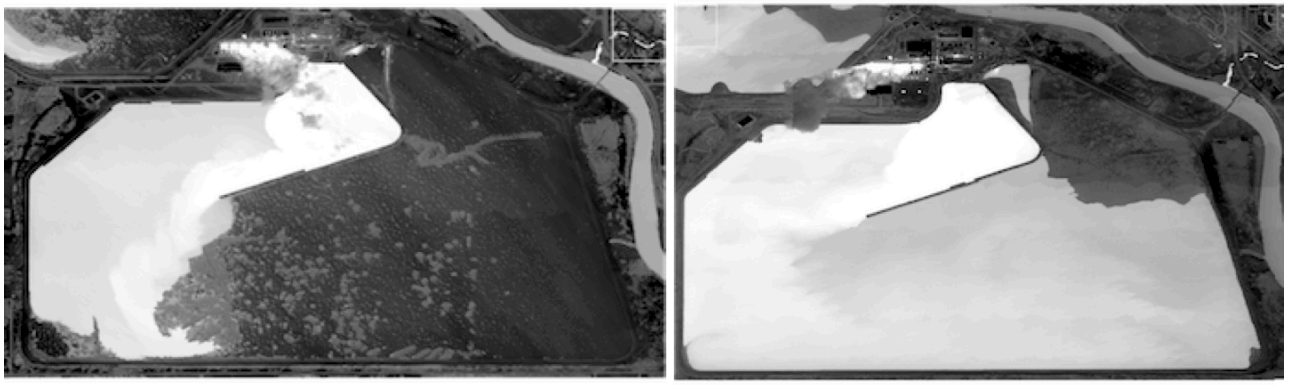

(a) Calibrated temperature map for 11 February 2010 collect (b) Calibrated temperature map for 4 March 2010 collect

Figure 10. Temperature maps. NOTE: There is a scale difference between both images

Shown in Table 1 are the mean-calculated variances for a section of approximately uniform water temperature as well as the amount of variation about that calculated mean. The data collected during the 4 March 2010 collection has a distinctly better accuracy which is directly attributable to quality of ground truth collected and the atmospheric homogeneity.

Show in Figure 11 are the collected surface temperatures for each day plotted against the correlating radiance values extracted from the sensor-reaching radiance mosaics. It can be seen that surface temperature data collected during the 4 March 2010 collect had a stronger linear relationship to the sensor-reaching radiance than the collected data from the 11 February 2010 collect.

Table 1. Statistics from uniform area of generated error maps

| Date | Mean $\sigma^2_{T_{cal}}$ | Standard deviation in $\sigma^2_{T_{cal}}$ |
|---|---|---|
| 11 February 2010 | 0.888863 | 0.015314 |
| 4 March 2010 | 0.248810 | 0.007750 |

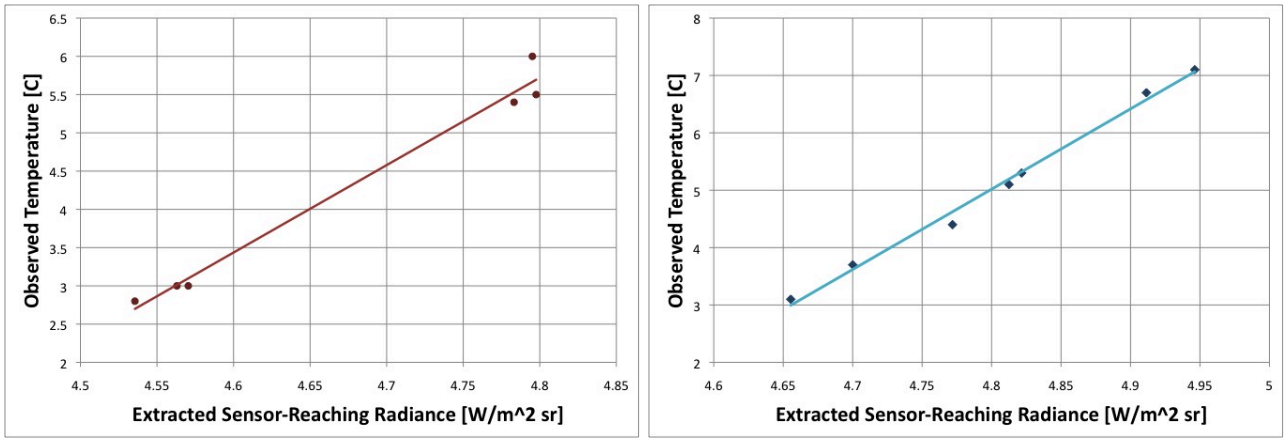


(a) 11 February 2010 (b) 4 March 2010

Figure 11. Radiance to ground temperature calibration model for both data sets

## 7. CONCLUSIONS

The notable variation between the two days ground data can be attributed to the strength of the linear fit generated for the translation between sensor-reaching radiance and ground observed temperature. The ground truth collected during the 4 March 2010 collect has a distinctly stronger linear relationship than the data collected for 11 February 2010 collect. As the linear fit between sensor-reaching radiance and ground observed temperature weakens, the error terms attributed to the linear model, $\sigma_{m_g}$ and $\sigma_{b_g}$, grow and as a result increase the magnitude of the derived variance.

This strong dependence on well fit ground truth data can be expected due to the linear assumption made regarding the relationship between radiance and temperature for a given target. Under that assumption, the atmospheric affects are believed to have a uniform, homogeneous affect on the emitted radiance from a given target; an affect that can accounted for by a simple gain and bias. As soon as the atmosphere between the WASP cameras and water surface becomes more spatially variant, this assumption deteriorates. For the particular environment observed for this research, the linear assumption does not consistently hold true. The body of water being observed has a highly varying thermal structure that produces a localized boundary layer micro-climate. In addition, the lake is accompanied by cooling towers, positioned on shore, which introduce a significant amount of moisture into the atmosphere. The presence of these phenomena are directly influencing the atmospheric make-up of the air column above the pond and can lead to a distinctly complicated radiometric environment.

There are periods of time where the influence from the cooling tower plumes are minimized (i.e. wind direction is favorable) and this particular calibration method produces adequate results, such as those presented above. In order to understand the true influence of the atmospheric effects, radiometric techniques need to be investigated and applied to the collected data sets. Continuing analysis of this data set included multi-altitude aerial imaging collections over the cooling pond. A multi-altitude compensation technique[6] will be applied to the data set in an attempt to determine atmospheric transmission and path radiance values. The effect of these new atmospheric parameters on derived ground temperatures can then be compared to the ground truth technique for validation.

In addition, there was also a time delay between aerial collection and ground data collection. It is possible that the time discrepancy introduced between measurements will also affect the linear model applied to the data. Further work can be performed to take advantage of the in-situ measurements recorded by the buoy systems. Querying the thermocouple closest to the surface of the water would provide a bulk temperature measurement acquired approximately (within a 5 minute interval) at the time of overflight. Collected bulk temperature

measurements would have to be converted to surface temperatures through a skin temperature compensation model. This approach is dependent on accurate weather reporting as well as having at least two buoys in open water during the time of overflight.

It is shown that near ideal collection conditions, as seen on March 4th 2010, the retrieval accuracy for water surface temperatures is $\pm 0.248810^{\circ}C$. A more complex environmental error introduces more error into the system, such as that observed during the February 11th 2010 collect. It can be concluded, that barring the introduction of an atmospheric compensation technique or more refined temperature retrieval method, the accuracy of derived thermal maps will be directly correlated to the quality of temperature measurements made on the ground and the atmospheric conditions at the time of acquisition.

## 8. ACKNOWLEDGEMENT

This work was carried out under funding received from the United States Department of Energy's Savannah River National Laboratory under contract number DE-A009-96SR18500. The collection of this data set is directly attributable to the collaboration with the Midland Cogeneration Venture in Midland, MI. All calibration software was developed in IDL and incorporated into the ENVI product provided to RIT as part of RIT's designation as a Geospatial Innovation Center for Excellence by ITT Visual Information Solutions.

## REFERENCES

1. A. J. Garrett, M. V. Arsenovic, and C. Salvaggio, "Thermodynamics of partially frozen cooling lakes," in *Proceedings of the SPIE, SPIE Defense and Security, Thermosense XXXI, Infrared Sensors and Systems*, **7299**, SPIE, April 2009.
2. A. J. Garrett, "Analyses of MTI imagery of power plant thermal discharge," *Imaging Spectrometry VII* **4480**, pp. 264–273, SPIE, Jan 2002.
3. A. J. Garrett and D. Hayes, "Cooling lake simulations compared to thermal imagery and dye tracers," *Journal of Hydraulic Engineering* **123**, p. 885, 1997.
4. M. V. Arsenovic, C. Salvaggio, A. J. Garrett, B. D. Bartlett, J. W. Faulring, R. L. Kremens, and P. S. Salvaggio, "Use of remote sensing data to enhance the performance of a hydrodynamic simulation of a partially frozen power plant cooling lake," in *Proceedings of the SPIE, SPIE Defense and Security, Thermosense XXXI, Infrared Sensors and Systems*, **7299**, SPIE, April 2009.
5. Y. Beers, *Introduction to the theory of error*, Jan 1957.
6. J. R. Schott, *Remote sensing: the image chain approach*, Jan 2007.